Supporting Material

Protein Signaling Networks from Single Cell Fluctuations and Information Theory Profiling

Young Shik Shin, [† § Δ] F. Remacle, [‖ Δ] Rong Fan, [‡‡] Kiwook Hwang, [† ‡] Wei Wei, [† ¶] Habib Ahmad, [† ‡] R. D. Levine [** ††] and James R. Heath [† ‡ *]

[†] Nanosystems Biology Cancer Center and Kavli Nanoscience Institute, [‡] Division of Chemistry and Chemical Engineering, [§]Division of Engineering and Applied Science, Bioengineering, [¶]Material Science, California Institute of Technology, 1200 East California Boulevard, Pasadena, CA 91125, USA

[‖] Département de Chimie, B6c, Université de Liège, B4000 Liège, Belgium

[**] The Institute of Chemistry, The Hebrew University of Jerusalem, Jerusalem 91904, Israel

[††] Crump Institute for Molecular Imaging and Department of Molecular and Medical Pharmacology, David Geffen School of Medicine, University of California, Los Angeles, CA 90095

[‡‡]Department of Biomedical Engineering, Yale University, PO Box 208260, New Haven, CT 06520, USA

[Δ] These authors contributed equally to this work.

*Correspondence: heath@caltech.edu (JRH)

Running Title: Proteins Fluctuations from Single Cell

The supporting matieral file has two main parts, 10 figures and 8 tables.

Supplementary Experimental Methods (SI. I) The experimental method and results.

Supplementary Theory Methods (SI. II) An outline of the theoretical methods.

Figure S1. Design of integrated microchip for single cell protein secretome analysis.

Figure S2. Cross-reactivity check and calibration curves.

Figure S3. Morphology change of THP-1 cells upon PMA/LPS activation and the cell viability test results.

Figure S4. Comparison of two data sets from two experiments performed in parallel.

Figure S5. PMA and LPS activation and kinetics of protein secretion from activated macrophage cells.

Figure S6. Simulated histograms of average intensity from multiple DNA barcode loctions.

Figure S7. The eigenvalues of the covariance matrix, for the experimental data of the main text, in order of decreasing magnitude from samples containing n =1 cells.

Figure S8. The dependence of the dominant eigenvalues of the covariance matrix on the number of cells in the sample.

Supplementary Experimental Methods (SI. I)

I. Experimental Procedure

***Microchip Fabrication*.** The SCBCs were assembled from a DNA barcode microarray glass slide and a PDMS slab containing a microfluidic circuit (1, 2). The DNA barcode array was created with microchannel-guided flow patterning technique (2). Each barcode was comprised of thirteen stripes of uniquely designed ssDNA molecules. PDMS microfluidic chip was fabricated using a two-layer soft lithography approach (3). The control layer was molded from a SU8 2010 negative photoresist (~20 μm in thickness) silicon master using a mixture of GE RTV 615 PDMS prepolymer part A and part B (5:1). The flow layer was fabricated by spin-casting the pre-polymer of GE RTV 615 PDMS part A and part B (20:1) onto a SPR 220 positive photoresist master at ~2000 rpm for 1minute. The SPR 220 mold was ~18 μm in height after rounding via thermal treatment. The control layer PDMS chip was then carefully aligned and placed onto the flow layer, which was still situated on its silicon master mold, and an additional 60 min thermal treatment at 80 °C was performed to enable bonding. Afterward, this two-layer PDMS chip was cut off and access holes drilled. In order to improve the biocompatibility of PDMS, we performed a solvent extraction step, which removes uncrosslinked oligomers, solvent and residues of the curing agent through serial extractions/washes of PDMS with several solvents (4, 5). We noticed that this step significantly improves the biocompatibility and the reproducible protein detection. Finally, the microfluidic-containing PDMS slab was thermally bonded onto the barcode-patterned glass slide to give a fully assembled microchip.

***Barcode Arrays*.** The barcode array initially consists of 13 uniquely designed DNA strands labeled in order as A through M. Prior to loading cells, a cocktail containing all capture antibodies conjugated to different complementary DNA strands (A'-L') is flowed through the chambers, thus transforming, via DNA-hybridization, the DNA barcode into an antibody array. These dozen proteins that comprised the panel used here were encoded by the DNA strands A through L, respectively. Calibration and cross reactivity curves for each protein assay are in Fig. S2, The DNA oligomer sequences and the antibody pairs used are listed in Tables S1 and S2.

Culture and stimulation of THP-1 cells. We cultured human monocyte THP-1 cells (clone TIB 202) in RPMI-1640 (ATCC) medium supplemented with 10% fetal bovine serum and 10 μM 2-mercaptoethanol. Cells grown close to the maximum density (0.8×10^6 cells/mL) were chosen for the experiment. Cells were first treated with 100 ng/mL phorbol 12-myristate 13-acetate (PMA) for 12 hours during which a characteristic morphological change was noticed as an indication of the induction to the macrophages (Fig. S3). Cells were washed with fresh media and resuspended in media with PMA (100 ng/mL) and lipopolysaccharide (LPS, 200 ng/mL) at 0.5×10^6 cells/mL for the further differentiation and the TLR-4 activation.

***On-chip secretion profiling*.** Prior to loading cells on chip, the DNA barcode array was

transformed into an antibody microarray through the following steps. First, 1% bovine serum albumin (BSA) in phosphate buffered saline (PBS) was flowed and dead-end filled into the chip to block non-specific binding. Second, a 200-μl cocktail containing all 12 DNA-antibody conjugates at 1.25 μg/mL in 1% BSA/PBS buffer was flowed through all microfluidic channels for a period of 1 h. Then, 100 μl of fresh buffer was flowed into the device to replace DNA conjugated primary antibody solutions. The chip is then ready for use. Cells stimulated with PMA/LPS were loaded into the SCBC chip within 10 min in order to minimize pre-loading secretion. Then, the pneumatic valves were pressed down by applying 15-20 psi constant pressure to divide 80 microfluidic channels into 960 isolated microchammbers. Next, the cells in every microchamber were imaged under a Nikon LV100 microscope and their numbers were counted. Afterwards the chip was placed in a cell incubator (~37 $^{\circ}$C and 5% CO_2) for 24 hours to perform on chip secretion. The chip was removed from the incubator and a 200 μl cocktail containing all detection antibodies (each at 0.5 μg/mL concentration) tagged with biotin flowed through the microchannels by releasing the valves. Then, 200 μl of the fluorescent probe solution (1 μg/ml Cy5-labeled streptavidin and 25 nM Cy3-labeled M' ssDNA) was flowed through to complete the immuno-sandwich assay. Finally, the PDMS slab was peeled off and the microarray slide was rinsed with 1×PBS, 0.5×PBS and DI water twice, sequentially, and spin-dried.

Bulk secretion profiling. Bulk measurements on the same panel of secreted proteins as were assessed within the SCBC microchambers were also carried out for the THP-1 cells with no stimulation, PMA stimulation, and PMA+LPS stimulation. Cells were cultured at 0.3×10^6 cells/mL, a comparable density to a single cell in a chamber. The media were collected after 24 hours and the secreted proteins were detected as described below. For the PMA+LPS stimulation condition, the media were collected at multiple time points (2, 4, 6, 8, and 10 hours) for the time-dependent analysis as well. For the bulk test, SCBC chip was utilized without using valves for the microchannel to microchamber conversion. The same conditions as for the on-chip secretion profiling were applied except for the cell incubation step. Instead, the collected media was introduced to the channel sets and incubated for 3 hours in the incubator.

Quantification and statistics. All the barcode array slides used for quantification were scanned using an Axon Genepix 4400A two-color laser microarray scanner at the same instrumental settings—50% and 15% for the laser power of 635 nm and 532 nm, respectively. Optical gains are 500 and 450 for 635 nm and 532 nm fluorescence signals, respectively. The brightness and contrast were set at 90 and 93. The averaged fluorescence intensities for all barcodes in each chamber were obtained and matched to the cell number by custom-developed MATLAB (The MathWorks, Natick, MA) codes. Heat maps were generated using Cluster 3.0 and Java *treeview* (http://rana.lbl.gov/EisenSoftware.htm).

II. Experimental Data Analysis Methods

***Conversion to the number of molecules*.** The collected raw data is based on the fluorescence. In order to convert the fluorescence to the number of protein molecules, we used the calibration curves (Fig. S2). We used the four parameter logistic model which is commonly used for fitting ELISA calibration curve. The fitting parameters can be found from the Table S5.

$$y = \frac{A_1 - A_2}{1 + (x / x_0)^p} + A_2$$

Signal- to- Noise Calculations. Since the signal range highly depends on the activities of the antibodies as well as the cell biology, it is required to decide if the signal is real and reliable. Certain assayed proteins were identified as positively detected from single cells based upon signal-to-noise ratio (S/N), which was measured as follows: For each microchamber, the averaged fluorescence from the two barcode stripes used to capture and detect a given protein and the averaged fluorescence from the barcode stripes designed to capture and detect IL-2 were obtained. The ratio of the averaged values over all single cell experiments (specific protein to IL-2) yields a S/N value. An S/N of 4 was utilized as a minimum for positive detection. Eight secreted proteins were thus identified from the single cell measurements. Those proteins were (with S/N included in the parenthesis after the protein name): MCP-1 (4.65), MIF (1381.13), IFN-γ (4.33), VEGF (77.32), IL-1β (94.70), IL-8 (2622.40), MMP9 (119.50), and TNF-α (410.74).

Analysis of experimental and biological variation from SCBC-based single cell measurement. One of the major characteristics of SCBC analysis is the heterogeneous cellular behavior at single cell level. The experimental variation of the SCBC platform which reflects the system error as well as the biological variation due to the cellular heterogeneity is contributing to the fluctuation of the total signal. Thus, we need to check if the heterogeneous signal responses are from the cells or the device itself.

The experimental error mainly includes the variation from non-uniform DNA barcode patterns and the variation due to the randomly distributed cell location in the chamber. The former one can be estimated by the histogram of the fluorescence intensity from the calibration experiment with recombinant proteins. Since the recombinant protein has fixed concentration over the entire channel, it represents a uniform protein level without any heterogeneity and location dependence. As a result, the distribution of the fluorescence intensity of a specific recombinant reflects the detection profile of the DNA barcode.

Fig. 1C shows a representative histogram of signal derived from recombinant MIF protein at 5 ng/ml. The histogram shows a nice Gaussian distribution with a coefficient of variation (CV) around 7%. In the calibration experiment, basically the intensities of all the recombinant proteins at detectable concentrations follow a Gaussian distribution with CVs typically lower than 10%.

The cell location is another important factor for the system error. Even though the chamber size is small, it is still big for a single cell. So the protein signal is dependent on diffusion and that is why the cell location can be a source of the variation. In order to minimize this effect, we utilized two sets of barcodes in a chamber and used the averaged signal intensity from two barcodes as the final signal value. However, the barcode close to the cell will undergo a higher local protein concentration than its counterpart and the different intensities of two sets of barcodes are amplified during the long incubation time. The diffusion process will lead the system close to the equilibrium but the cell that keeps secreting proteins with different kinetics makes it difficult for the chamber to reach its full equilibrium. In that sense, the randomly located cells can add an extra uncertainty to the SCBC system.

Because it is difficult to isolate the system error (especially for the cell location effect) from the heterogeneous cell response experimentally, we performed a Monte Carlo simulation by R (R Foundation for Statistical Computing, version 2.10.1). First of all, we investigate the case of MIF as a representative case. We assumed one chamber has two sets of 13 barcodes such that all of them have MIF antibodies. By randomly positioning a cell with a fixed protein secretion rate and getting the protein concentration at specific barcode positions, we can find out what is the variation that purely depends on the cell location and barcode non-uniformity. The total amount of secreted MIF during 24 hours was estimated based on our experimental result. The secretion rate was 4.84 pg/mL per min from the SCBC (used for the simulation) and 11 pg/mL per min from the bulk condition. The corresponding secretion rate of a single cell, back-calculated based on the chamber and cell size ($10\mu m^3$), was 0.065 nM/min. Values of parameters used in simulation can be found from Table S6. 5000 data sets for the protein concentration distributions from randomly located single cell were generated by solving a diffusion equation with a custom made MATLAB code and the results were analyzed with R. The parameters used in the simulation are exactly the same as our experimental environment. The chamber is 2000 μm in length and 100 μm in width with two sets of DNA barcodes M-A and A-M from left to right. Each barcode is 20 μm in width with 50 μm in pitch (30μm gap between barcodes). The detection variation of the MIF protein due to the DNA uniformity obtained from the histogram of the calibration data set was incorporated to the analysis. Fig. 1E shows the histogram of the average fluorescence intensity from DNA sequence E (corresponding to MIF in the actual experiment) for 5000 single cell cases. For the barcode variability, the actual value of 7.3% was used. The final system error was 5.1% which is a lot smaller than the assay error from the experimental data sets, 55.2 %.

In order to think of the worst case, we used the barcode variability of 10% for the rest of the analysis. If the cell location effect is significant, we are supposed to see different errors on different barcode positions. Fig. S6 illustrate the histograms of average intensities from multiple barcode locations. The blue curves are line profiles of Gaussian distribution fitted with the mean and the standard deviation obtained from the corresponding simulation. The nice fitting between the Gaussian

curves and the histogram indicates that the average intensity per chamber follows a Gaussian distribution with a predictable mean and CV. The CVs from this simulation represent the distribution of our measurements for single cell chambers without considering the cellular heterogeneity, i.e. the system error. The experimental CVs for different barcode locations based on the system error were quite similar to one another (~ 7%).

We can define CV_{system} as the system error estimated by the simulation. We can also calculate the assay error from our experimental data set such that CV_{assay} refers to the total CV of our experimental data. Consequently, the biological variation for single cell experiment can be quantitatively estimated by the formula below:

$$CV_{\text{assay}} = (CV^{2}{}_{\text{system}} + CV^{2}{}_{\text{biological}})^{1/2}$$

An estimation of biological variations of proteins for different barcode locations are shown in Table S7. It can be noticed that the biological variation is dominant in the total error of the assay. This analysis verifies that the signal fluctuation that we can see from the single cell experiment is a good representation for the single cell heterogeneity rather than the systemic error from our platform.

Supplementary Theory Methods (SI.II)

I. Introduction to theoretical supplementary methods

We show how to characterize protein-protein interactions. Specifically we show (*i*) that the different tiers of a signaling network can be quantitatively determined from the measured fluctuations in the concentrations of signaling proteins and (*ii*) that the measured fluctuations in the concentrations of signaling proteins for the unperturbed cell can be used to predict the effect of introducing perturbations such as neutralizing antibodies. The approach is developed from an information theoretic perspective and it is related to the specification of the direction of change when a system responds to a perturbation, known as the principle of Le Chatelier. The corresponding result here is that we predict the sequence of tiers in the network, see Fig. 4 of the article. In addition we specify which signaling proteins are at a given tier of the network and their mutual influence including inhibition, see Fig. 5 of the article. Experimental measurements of the fluctuation of concentrations in samples with nanoliter volume containing n cells, n = 0,1,2,.. , see Fig. S8 below, are used to validate the signaling protein network. Finally we use the protein-protein interaction as determined for the unperturbed cell to quantitatively predict, Fig. 6 of the article, the effect of perturbations.

The approach we propose provides an analogue and an extension of the statement that heat is transferred from a warmer to a colder body. We can understand this statement as a statement about the direction of a process between two equilibrium states, meaning that it is a

static principle. We can also think of it as a statement about the dynamics, meaning that it specifies the rate of change. We will here develop the formalism for the static interpretation. The explicit introduction of time is possible and we have the required formalism at hand but it requires a more elaborate theoretical foundation and so will be given elsewhere.

II. The ensemble: a basis for making predictions

The system we consider is many independent replicas of a compartment containing a single cell in a nutrient solution at thermal equilibrium. Because the system is not large, different replicas of it can differ in the number, N_i, of secreted proteins of kind *i*. We seek to represent these fluctuations by taking the different replicas as different samples from an ensemble of single cell compartments where the mean number $\bar{N}_i$ of proteins of kind *i* over the ensemble is given. Another given quantity is the energy, (and volume that we do not indicate explicitly). We now seek the most probable distribution of protein numbers in different compartments. The solution is well known because if many compartments are measured then the required distribution is the one whose entropy is maximal. In textbooks of statistical mechanics this search for the most probable distribution is sometime called the Boltzmann approach. It is possible to show (6) that this approach does not require the system to be macroscopic in size. It is sufficient if we measure enough replicas so that the distribution of proteins does not significantly change as we add more measurements. If each replica is macroscopic the fluctuations will be small and rare. Repeated measurements will give the same results. If each replica is small we can observe the fluctuations, which is the experiment described in the main text.

The key point is that even if the fluctuations are not small it is possible to make predictions. We discuss three types of predictions in the paper, with more details given in this section of the SI. We predict the distribution of fluctuations, we predict the tiers in the network and, in particular and as shown in Fig. 6 of the main text, we predict the response of a system to a perturbation. For these first and last predictions, we compare directly with experimental results. We emphasize that the prediction is made strictly independently of the experiment to which it is compared.

The probability of a system in a particular composition can be shown to be given by

$$P(N_1, N_2, ..) = \exp\left\{\beta\left(\sum_i \mu_i N_i - E\right)\right\}\Big/\Xi \qquad \text{(S1)}$$

This straightforward result is perhaps misleading in its simplicity. It is most directly derived by the method of Lagrange undetermined multipliers. The numerical value of these multipliers is determined at the final stage by imposing the condition that the distribution (Eq. S1) reproduces the given values of the means. There are as many multipliers as conditions.

β is the Lagrange multiplier that is determined by the mean value of the energy and, as usual, is related to the temperature T as $\beta = 1/kT$ where k is Boltzmann's constant. The μ_i's are the chemical potentials as introduced in the thermodynamics of systems of more than one component (7, 8). The Lagrange multipliers that correspond to the given (mean) number of species i are known as the Planck potentials and denoted as α_i. It is often more convenient to work with μ_i, $\alpha_i = \beta\mu_i$. If our system were macroscopic in size we would call μ_i 'the chemical potential of protein i'. For convenience we retain the designation 'potential' because, as we shall show, μ_i retains essential properties of the chemical potential even when fluctuations are finite. Ξ is a function of all the Lagrange multipliers and its role is to insure that the sum of the probability over all possible compositions yields one.

There are at least two points where important details are not revealed by the notation used in Eq. S1. Both are relevant in what follows. First is the condition that the numerical values of the chemical potentials are determined by the given mean numbers, the $\bar{N}_i$'s, of the proteins. Strictly speaking, we should write the chemical potentials as functions of the $\bar{N}_i$'s. The other point arises when we want to treat the actual numbers N_i's of the different proteins as continuous variables. This is needed, for example, to compute averages, normalize the distribution (Eq. S1), etc. The integration for each protein is over $dN/N!$ where $N!$, the factorial of N, arises to account for the Gibb's paradox. Therefore, as a function of the continuous variable N the distribution for, say, one protein is

$$P(N) \propto \left(Q^N / N!\right) \exp(-\beta\mu N) \qquad \text{(S2)}$$

Here Q is the factor that arises by summing over all the internal states of the protein that are occupied at the temperature T. This result is used in the main text to fit the observed distribution for a single protein (Fig. 3).

III. Fluctuations describe the response to small perturbations.

We show that by measuring the fluctuations in the unperturbed system we can predict how the system responds to small perturbations (7). Proof: Say that we make a small change in the value of the chemical potential μ_i from its current equilibrium value to some new value $\mu_i + \delta\mu_i$. We do so isothermally. This change in μ_i potentially changes the equilibrium mean concentration of all species from $\bar{N}_j$ to $\bar{N}_j + \delta\bar{N}_j$, for all *j*. To compute the change in concentrations we need to consider the change in the ensemble as represented by Eq. S1. In the algebraic developments in Eq. S4 below we make use of the definition of the mean concentration

$$\bar{N}_j = \sum N_j P(N_1, N_2, ..) \tag{S3}$$

The summation in Eq. S3 is over all the possible compositions, each weighted by its probability $P(N_1, N_2, ..)$ computed as the distribution of maximal entropy. The same meaning for the summation is used also in Eq. S4 below. We denote this averaging by an over bar. From Eq. S1, the variation of the distribution that occurs when a particular chemical potential is changed by a small amount is $\delta P(N_1, N_2, ..) = \beta\delta\mu_i \; N_i P(N_1, N_2, ..)$. Note that it is in using this lowest term in the Taylor series that we assume that the change is small. It follows that on the average the proteins respond to the change as:

$$\begin{aligned}
\delta\bar{N}_j &= \sum N_j \delta P(N_1, N_2, ..) \\
&= \sum \left(N_j - \bar{N}_j\right)\delta P(N_1, N_2, ..) \\
&= \beta\delta\mu_i \sum \left(N_j - \bar{N}_j\right) N_i P(N_1, N_2, ..) \\
&= \beta\delta\mu_i \sum \left(N_j - \bar{N}_j\right)\left(N_i - \bar{N}_i\right) P(N_1, N_2, ..) \\
&= \beta\delta\mu_i \overline{\left(N_j - \bar{N}_j\right)\left(N_i - \bar{N}_i\right)}
\end{aligned} \tag{S4}$$

Note that the conservation of normalization implies that the average change in the probability must be zero, $0 = \sum \delta P(N_1, N_2, ..)$ and we have used this result in the derivation above. In the last line in Eq. S4 we have avoided writing the summation over all compositions by the use of the over bar to designate an average over the probability $P(N_1, N_2, ..)$, which is the notation introduced in Eq. S3.

Taylor theorem states that, in the leading order, the change of a function is the sum of the changes. Therefore the expression for an isothermal variation in all the chemical potentials leads to a change of the distribution of the form:

$$\delta P(N_1, N_2, ..) = \beta \sum_i N_i P(N_1, N_2, ..) \delta \mu_i \quad \text{(S5)}$$

The summation in Eq. S5 is an ordinary sum over the finite number *S* of signaling proteins, $i = 1, 2, .., S$. Then we have the general equation of change that is an extended form of Eq. S4 valid for all possible small isothermal changes in the chemical potentials

$$\delta \bar{N}_j = \beta \sum_i \overline{\left(N_j - \bar{N}_j\right)\left(N_i - \bar{N}_i\right)} \, \delta \mu_i \quad \text{(S6)}$$

This is the result that we use in this paper.

IV. The principle of Le Chatelier

The principle in its simplistic statement claims that the system responds to a perturbation in a direction that restores equilibrium. For example, when the temperature of a heat bath is increased the mean energy of an immersed system goes up so that the distribution remains canonical. The proof for our case starts from Eq. S3. When the chemical potential of protein *i* is changed, for an ensemble at maximal entropy the mean value of protein *j* changes by

$$\frac{\partial \bar{N}_j}{\partial \mu_i} = \sum N_j \frac{\partial P(N_1, N_2, ..)}{\partial \mu_i} \quad \text{(S7)}$$

where, as emphasized in Eq. S3, the distribution $P(N_1, N_2, ..)$ is not arbitrary but is the one of maximal entropy as exhibited in Eq. S1. Eq. S4 is recovered when the derivative in Eq. S7 is evaluated. The reader may feel that this is a triviality but it is not without meaning. What we have proven is that computing a small change in the distribution $P(N_1, N_2, ..)$ when a particular chemical potential is changed from the value μ_i to a new value $\mu_i + \delta\mu_i$ is the same as computing the derivative of the distribution $P(N_1, N_2, ..)$ at the point where the value of the chemical potential is μ_i . Then the change in the distribution is $\left(\partial P(N_1, N_2, ..)/\partial \mu_i\right)\delta\mu_i$. Of course, this is what differential calculus is about. Yet the result is not pure mathematics. It shows that the new distribution is a distribution of maximal entropy of the functional form Eq. S1 as otherwise the result will not hold. It says that a small change in the chemical potential μ_i, and no other change, leads to a new distribution which is also one of maximal entropy.

Typically we do not see the theorem of Le Chatelier stated as in Eq. S6. This is because of the practical point that the number fluctuations are typically not easy to observe in

a macroscopic system. Here however we deal with secretion of proteins by a single cell and, as shown in the main text and particularly in the histogram in Fig. 3, the distribution is clearly observed and the covariance can be computed from the experimental data as long as that the number of replicas is not small.

V. The equation for the direction of change

The (symmetric) square matrix $\overline{\left(N_j-\bar{N}_j\right)\left(N_i-\bar{N}_i\right)}$ is the covariance matrix of the (equilibrium) fluctuations in the (equilibrium) concentrations, the $\bar{N}_j$'s. It is an equilibrium average because, as explicitly shown in Eq. S4, it is an expectation over the equilibrium distribution as given in Eq. S3. The covariance matrix has the dimensions of *S* by *S* where *S* is the number of signaling molecules that take part. In practice we have to compromise on this definition meaning that *S* is the number of signaling molecules that can be detected. If an important protein is not detected then the network that we infer will be incomplete.

A covariance matrix can be shown to be a non-negative matrix, also called semipositive definite, meaning that its eigenvalues are zero or positive. If the concentrations of the signaling proteins can in principle be varied independently, which is definitely not necessarily the case, then the covariance matrix $\overline{\left(N_j-\bar{N}_j\right)\left(N_i-\bar{N}_i\right)}$ is a positive matrix with positive eigenvalues. We will discuss below why it will often be the case that for reasons of both principle and practice (e.g., experimental noise) there will be eigenvalues that are effectively zero. In that case, technically, the covariance matrix is positive semidefinite (9).

Eq. S6 specifies how the concentration of the *j*'th signaling molecule varies when the *i*'th chemical potential is changed. In general the correlation coefficient $\overline{\left(N_j-\bar{N}_j\right)\left(N_i-\bar{N}_i\right)}$ between the signaling molecules *i* and *j* can be either positive or negative. Therefore, in general the change $\delta\bar{N}_j/\delta\mu_i$ is not necessarily of the same direction for all proteins *j*. This obvious result will be important for us below. Using the observation that the covariance matrix is semipositive definite, it is however possible to determine the direction of change by first diagonalizing the covariance matrix. This means that we can determine *S* distinct linear combinations of signaling molecules, where (*a*) each such set of molecules changes in a given direction and (*b*) we can order the different sets in terms of the extent of their response such that the first set is the most changing, the second set changes to a lesser extent, etc. In

the time dependent formalism, not presented here, we can outright say that the first set is the fastest changing and therefore it is the first to change. Then there follow changes in the second set, etc. It is clearly our intention to identify each set of signaling molecules as the set of molecules in a given tier in the network.

VI. Tiers of the network are eigenvectors of the correlation matrix

Our next purpose is to define the tiers of the network. The set of proteins that participate in the *m*'th tier is determined as follows. Let $\mathbf{S}_m$ designate the *m*'th eigenvector of the covariance matrix where the eigenvectors are listed in order of decreasing magnitude of the corresponding eigenvalue. The largest eigenvalue is m =1. Each eigenvector $\mathbf{S}_m$ is a (column) vector of *S* components and it is determined by the matrix equation

$$\mathbf{\Sigma}\,\mathbf{S}_m = \sigma_m^2\,\mathbf{S}_m \quad , \; m = 1, 2, . \tag{S8}$$

where $\mathbf{\Sigma}$ is the *S* by *S* symmetric covariance matrix whose elements are $\mathbf{\Sigma}_{ij} = \overline{\left(N_j - \bar{N}_j\right)\left(N_i - \bar{N}_i\right)}$ and we explicitly indicated that the eigenvalues are positive or zero but not negative (which defines a positive semidefinite matrix). The eigenvectors of the symmetric covariance matrix are orthogonal to one another and can be chosen to be normalized

$$\mathbf{S}_{m'}^T \cdot \mathbf{S}_m = \begin{cases} 0, & m' \neq m \\ 1, & m' = m \end{cases} \tag{S9}$$

Here the superscript *T* designates the transpose so that $\mathbf{S}_{m'}^T$ is a row vector and Eq. S9 is the scalar product.

For each value of the number of cells, *n*, in the compartment the eigenvalues are arranged in the order of decreasing magnitude the largest eigenvalue being labeled as m =1 and the smallest as m =12 and the results are shown for n =1 in Fig. S7. See Fig. S8 for the dependence of the largest eigenvalues vs. cell number.

VII. The spectral representation of the covariance matrix.

Fig. 5 of the text shows the covariance matrix computed for experiments with one cell in the compartment. Table S8 is a digital representation of the same matrix.

Also shown in Fig. 5 is the resolution of the covariance matrix into tiers defined as follows. From each eigenvector $\mathbf{S}_m$ we can define an *S* by *S* symmetric matrix $\mathbf{P}_m$ as follows

$$\mathbf{P}_m = \mathbf{S}_m \cdot \mathbf{S}_m^T \qquad \text{(S10)}$$

The spectral theorem (10) is the result that the covariance matrix $\mathbf{\Sigma}$ can be resolved into tiers as

$$\mathbf{\Sigma} = \sum_m \sigma_m^2 \mathbf{P}_m \qquad \text{(S11)}$$

The eigenvalues σ_m^2 are arranged in a decreasing order so that each subsequent tier makes a smaller contribution. Fig. S7 shows that the eigenvalues decrease quite rapidly with increasing value of *m*. The very dominant contribution is from *m* =1 The leading eigenvalue = tier 1, is only about 30% bigger than the second one, *m* =2. The third eigenvalue is smaller by almost two orders of magnitude. Fig. S8 is a plot on a logarithmic scale of all non zero eigenvalues. There are only two eigenvectors that, judging by the value of their corresponding eigenvalues are definitely above the noise. The dominant (*m*=1) and the *m* = 2 eigenvectors for 1 cell measurements are shown in Fig. 5 of the text and for three cells in Fig. S9 below.

VIII. The role of the number of cells in the sample

It was possible to make repeated measurements of the protein concentrations for different values of the number of cells in the sample. In this section we argue that the direction of increasing *n* can be semi-quantitatively regarded as a direction of increasing time. Therefore by examining how the eigenvectors of the covariance matrix change with *n* we have an independent determination of the direction of the *dynamic* response of the system.

Fig. S8 shows are the largest eigenvalues for *n* = 0, 1, 2, 3 and 4 cells.

To interpret Fig. S8 within the point of view as used in this paper we argue as follows. A single cell secretes a number of different signaling proteins and therefore even the data measured for a single cell can show the role of protein-protein interactions. If two cells are in the sample these interactions increase in importance. If we think of *n* as a measure of concentrations of proteins then $\overline{N} \propto n$ but to compute the covariance we need to divide by the number of protein molecules. So for both paracrine and endocrine signaling we expect the covariance to increase with *n*. When *n* becomes high there may be three or more cells interacting and the simple considerations break down.

IX. Antibody perturbations

Fig. 6 shows a quantitative comparison of the measured results as compared to the purely theoretical prediction when neutralizing antibodies for specific proteins are added. We emphasize that it is a prediction because the results shown are based on using Eq. S4 that we repeat here:

$$\delta \bar{N}_j = \beta \overline{\left(N_j - \bar{N}_j\right)\left(N_i - \bar{N}_i\right)} \delta \mu_i = \beta \boldsymbol{\Sigma}_{ji} \delta \mu_i$$

The addition of a neutralizing antibody for protein i means that $\delta \mu_i$ is negative. The entries for the matrix $\boldsymbol{\Sigma}$ are given in Table S3. This matrix is computed for the unperturbed data. It is the matrix given in the table above that gives rise to the theoretical results shown in Fig. 6. We emphasize that the experimental results shown in Fig. 6 are for single cells in the compartment. This means, see Fig. S8 that the largest eigenvalue, $\sigma^2_{m=1}$, of the covariance matrix is large indeed. Then, from Eq. S11, the contribution from the first tier dominates. It is the two proteins in this tier that are shown in the panel. There are bigger discrepancies between theory and experiment for tiers 2 or 3 for which the experimental signal is weak.

Supplementary Figures

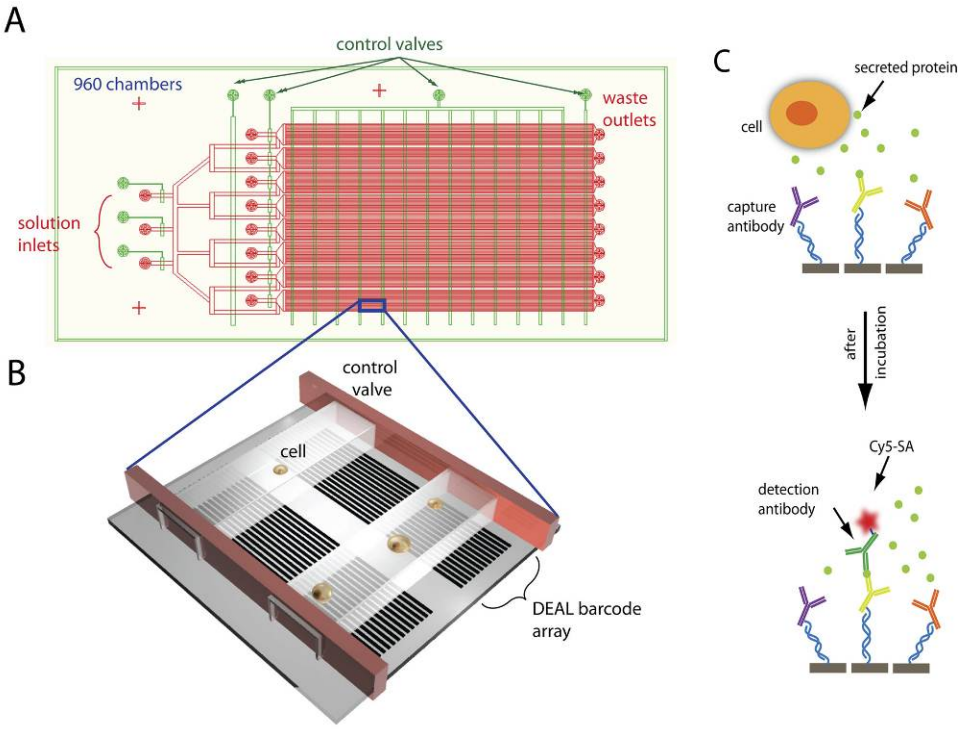

Figure S1. Design of integrated microchip for single cell protein secretome analysis. (A) CAD design of a microchip in which flow channels are shown in red and the control channels are shown in green. (B) Schematic drawing of cells loaded in the microchambers and compartmentalized with the valves pressurized. (C) Schematic illustration of the antibody barcode array used for multiplexed immunoassay of single cell secreted proteins.

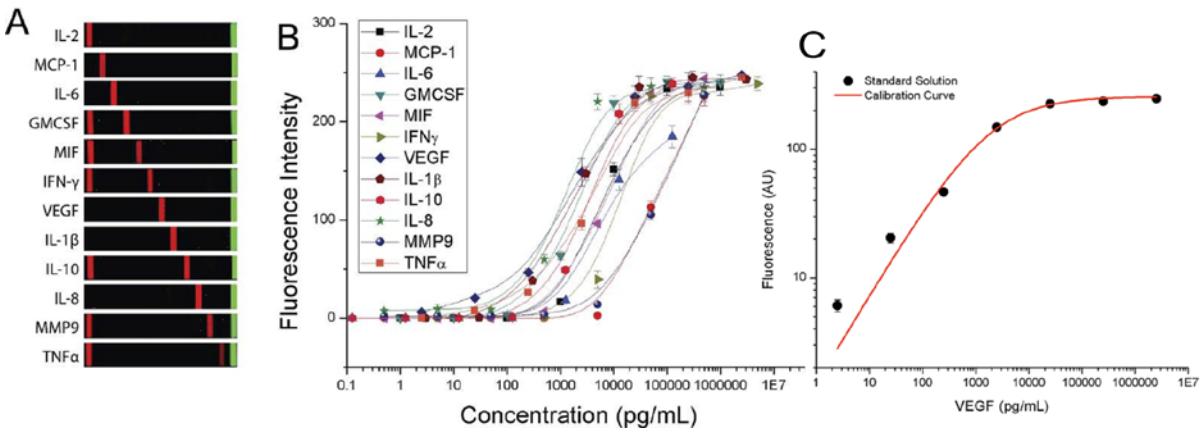

Figure S2. Cross-reactivity check and calibration curves. (A) Scanned image showing cross-reactivity check for all 12 proteins. The green bars represent the reference stripe, sequence M. Each protein can be readily identified by its distance from the reference. In each channel, a standard protein (indicated on the left) was added to the buffer solution and assayed using the DEAL barcode method. For GMCSF, MIF, IFN-γ, IL-10, MMP9, and TNF-α, biotin-labeled 2° anti IL-2 antibody conjugated to DNA sequence A' was used as a control. (B) Quantitation of fluorescence intensity vs. concentration for all 12 proteins. Error bars: 1SD. The variability (defined as the standard deviation divided by the average in percentage) is less than 10% for the signals in detectable range. (C). Plot of the same VEGF calibration data as in (B), but presented as a log / log scale, which may be more familar to some readers.

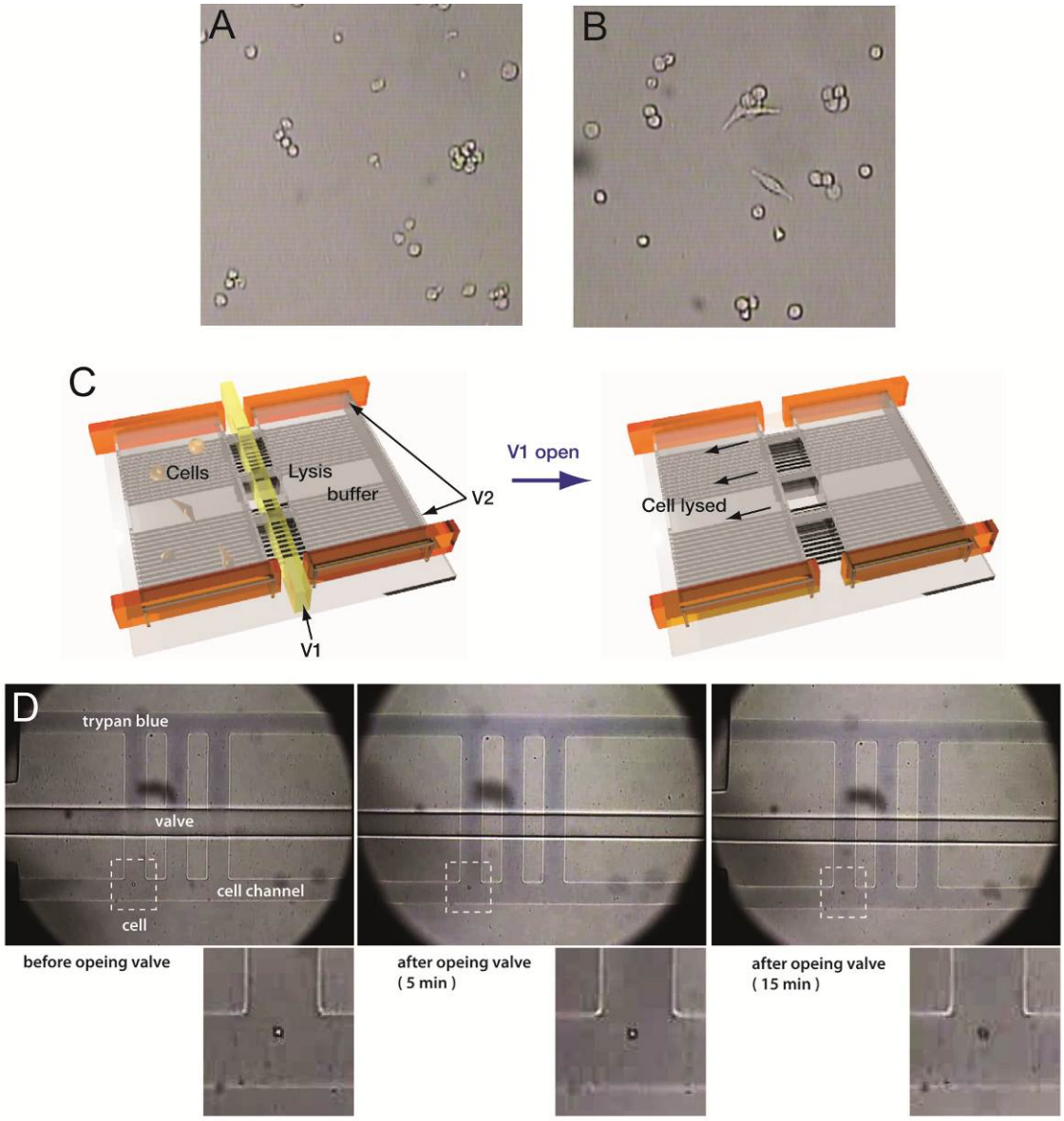

Figure S3. Morphology change of THP-1 cells upon PMA/LPS activation for 24 hours, and on-chip cell viability assay. (A) monocytic THP-1 cells without induction, (B) macrophage-like THP-1 cells after PMA/LPS treatment. The morphological change from non-adherent to adherent phenotypes was observed upon PMA/LPS treatment. (C) Schematic illustration of the device for cell viability test. The device has two parallel channels connected through three interconnecting channels. One channel is used for cell loading and the other channel is filled with trypan blue. Valve set V1 separates the cell loading channel and the trypan blue channel. Valve set V2 is for converting channels into chambers. After 24 hours of incubation, valve set V1 opens and trypan blue mixes with the cell media by diffusion. The cell viability is checked by the color change of the cells. (D) A representative picture of the cell viability test result. 5 min (sufficient time for diffusion mixing) after valve opening, a cell still doesn't get stained, which indicates cells can survive for 24 hours in the microfluidic device. After long exposure (15 min) to the trypan blue, cell color changes into dark blue due to the toxicity of trypan blue.

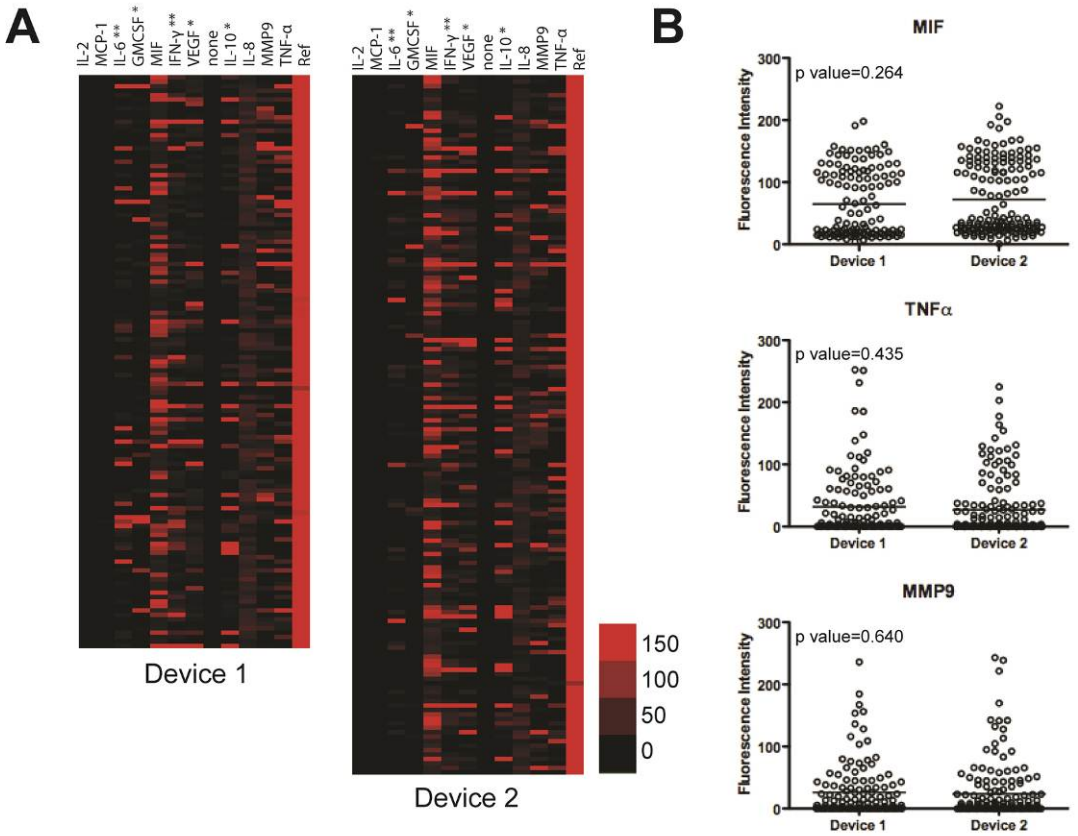

Figure S4. Comparison of two data sets from two experiments performed in parallel. All the conditions such as barcode patterning, PDMS-based microfluidic device fabrication, and cell preparation etc for the two devices were the same. (A) Heat maps of the single cell data sets from two devices. Based on the same S/N ratio (4), 9 proteins were detected. It should be noted that the protein profiles are different from the data set used in the main text, which was originated from the non-extracted PDMS device. PDMS is known to leach out toxic material to the solution and this can affect to the cell condition or protein secretion because macrophages are, by nature, highly responsive to their environment. For the main experiment, solvent-extracted PDMS was used to avoid such effects. For some proteins, the signal values are multiplied by 10 (*) and 100 (**) for the visualization (B) Dot plots for three major proteins. Based on p-values, it can be found that both experimental data sets are statistically close to each other.

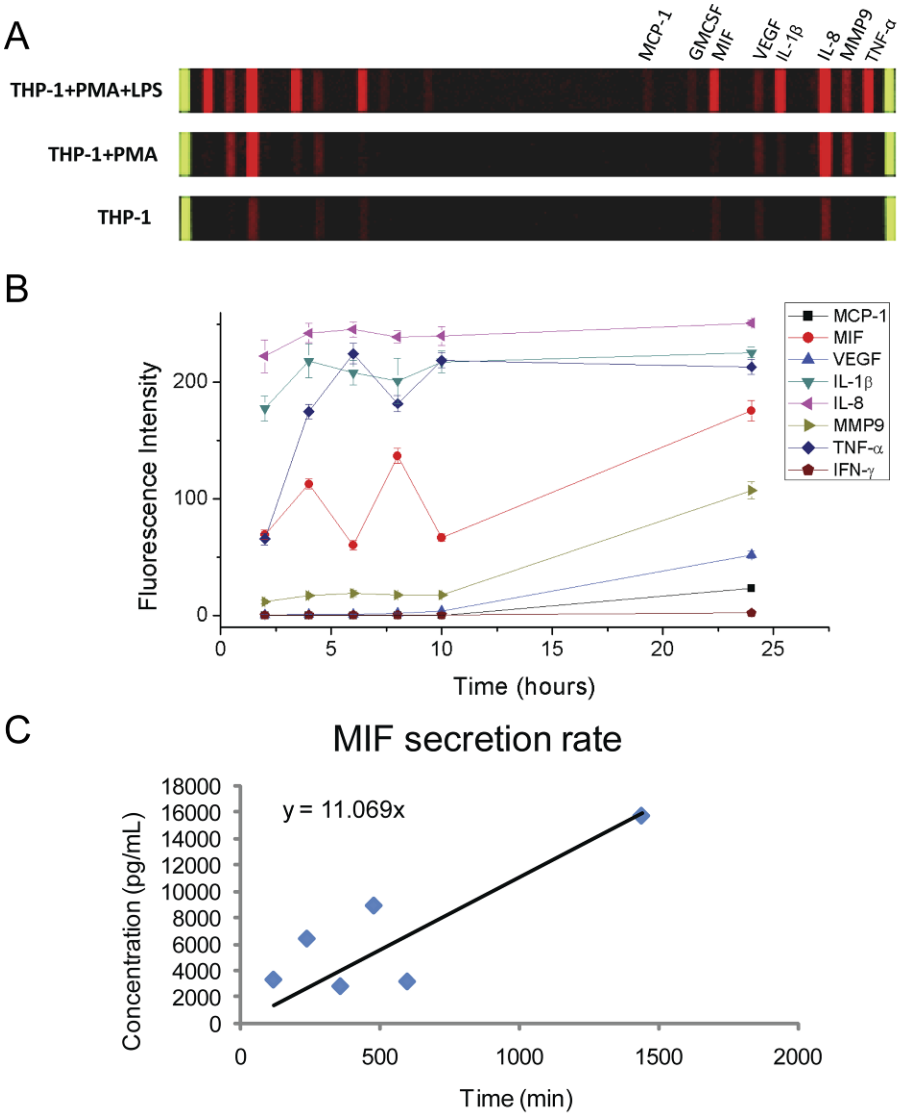

Figure S5. PMA and LPS activation and kinetics of protein secretion from activated macrophage cells. (A) Bulk secretion profiles from THP-1 cells under different conditions. PMA treatment induces THP-1 cells to macrophages and LPS treatment emulates innate immune responses against Gram-negative bacteria (B) Quantitation of bulk secretion intensities for the eight selected proteins over 24 hours. The samples were collected at 2, 4, 6, 8, 10, and 24 hours after incubation of PMA/LPS treated cells. The cell density was 0.3×10^6 cells/mL, which is a comparable density to a single cell in a chamber of SCBC device. Note that the secretion levels of TNF-α and MIF are oscillatory and anti-correlated. (C) MIF secretion rate based on the assumption of linear time dependence from (B). The secretion rate from the bulk experiment is about 11 pg/mL per min which is about two fold higher than the single cell secretion data from the SCBC device (4.84 pg/mL per min).

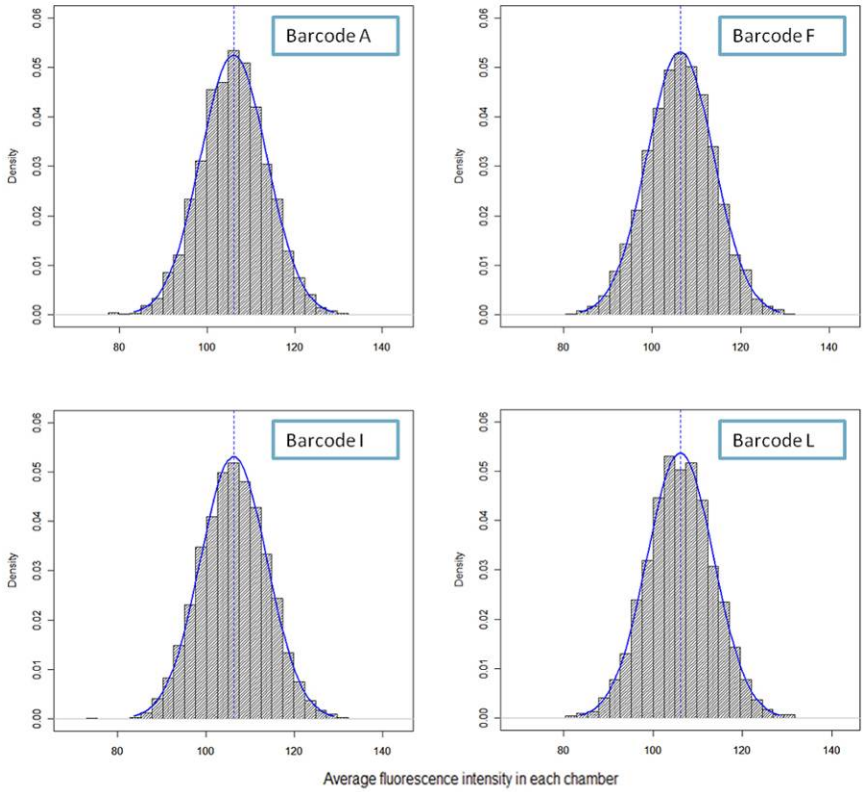

Figure S6. Simulated histograms of average intensity from multiple DNA barcode loctions. The signal intensities for 5000 single cell data set were obtained by solving a diffusion equation for a randomly located cell. For the barcode variability, the value of 10% was used. The blue curves are the Gaussian fitting of the histogram with sample mean and sample standard deviation from the simulation.

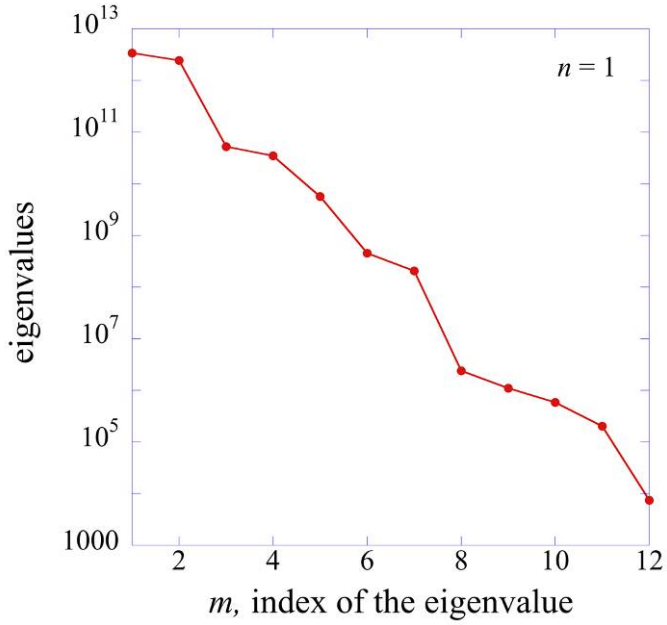

Figure S7. The eigenvalues of the covariance matrix, for the experimental data of the main text, in order of decreasing magnitude for samples containing n =1 cells.

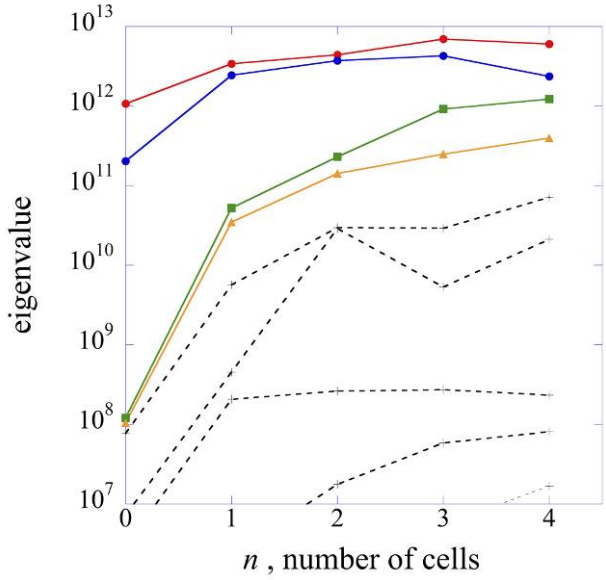

Figure S8. The dependence of the dominant eigenvalues of the covariance matrix on the number of cells in the sample. The result for n = 0, the backgound, is included to show the influence of the noise. The dashed lines, the fifth and higher eigenvalues are more corrupted by noise.

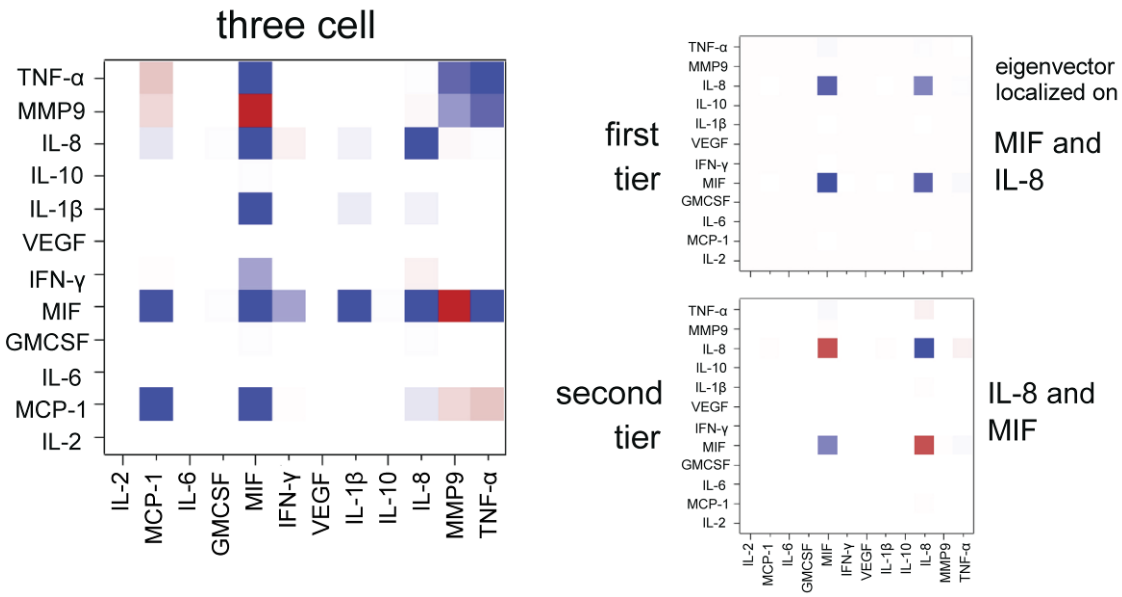

Figure S9. Heat map of the covariance matrix (left) and of the contributions to the first two tiers of the network (right) for measurements on chambers containing 3 cells. Similar to the single cell case (Fig. 5), the entries in the tiers are scaled by the size of the eigenvalues. See the spectral representation of the covariance matrix, Eq. S11. The plot at left is the covariance matrix computed from the observed fluctuations in the 3-cell data. The color code is -8e+10 (red) to 0 (white) to +8e+10 (blue). The range is fixed so as to attenuate the effect of the self terms in the covariance matrix. For tier 1 and tier 2, the ranges are [-4.3e-12, 4.3e+12] and [-7e+10,7e+10] respectively. Note that when the numbers of cells per chamber increases, anti-correlations can get washed out.

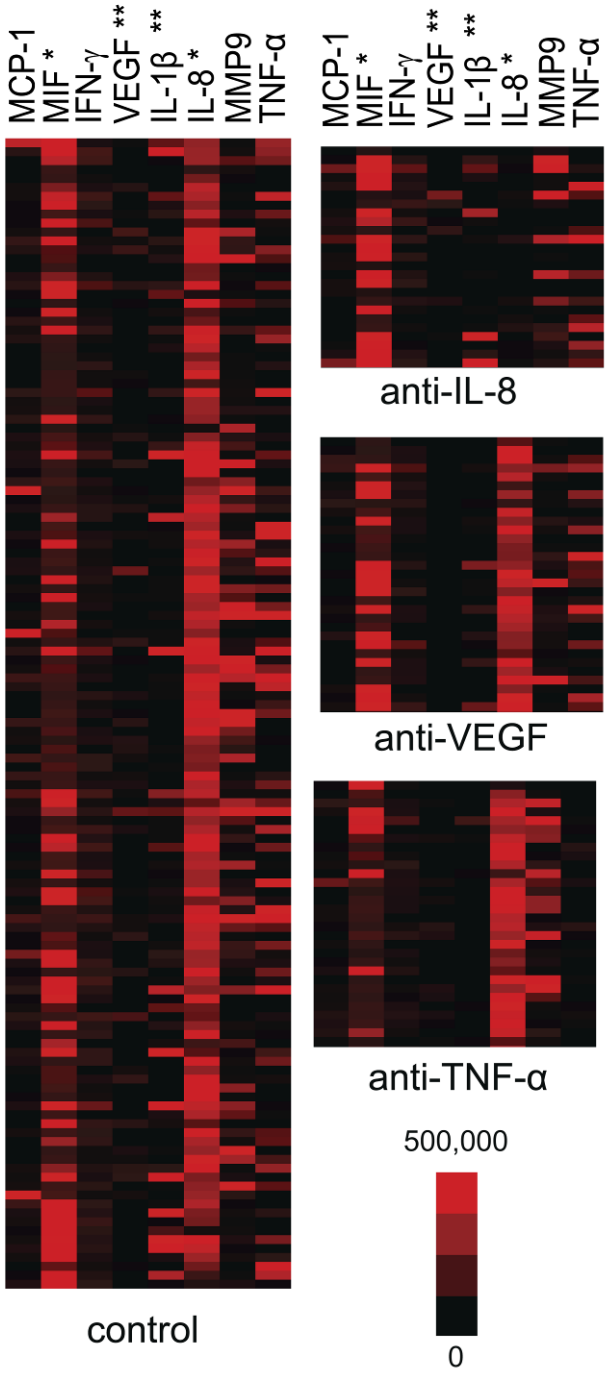

Figure S10. Heat map plots showing the secretion profiles of single cells when adding different neutralizing antibodies. For visualization, signals are decreased and amplified 10× for * and **, respectively.

Supplementary Tables

Table S1. Sequences and terminal functionalization of oligonucleotides*.

Name	Sequence
A	5'- AAA AAA AAA AAA AGT CCT CGC TTC GTC TAT GAG-3'
A'	5' NH3-AAA AAA AAA ACT CAT AGA CGA AGC GAG GAC-3'
B	5'-AAA AAA AAA AAA AGC CTC ATT GAA TCA TGC CTA -3'
B'	5' NH3-AAA AAA AAA ATA GGC ATG ATT CAA TGA GGC -3'
C	5'- AAA AAA AAA AAA AGC ACT CGT CTA CTA TCG CTA -3'
C'	5' NH3-AAA AAA AAA ATA GCG ATA GTA GAC GAG TGC -3'
D	5'-AAA AAA AAA AAA AAT GGT CGA GAT GTC AGA GTA -3'
D'	5' NH3-AAA AAA AAA ATA CTC TGA CAT CTC GAC CAT -3'
E	5'-AAA AAA AAA AAA AAT GTG AAG TGG CAG TAT CTA -3'
E'	5' NH3-AAA AAA AAA ATA GAT ACT GCC ACT TCA CAT -3'
F	5'-AAA AAA AAA AAA AAT CAG GTA AGG TTC ACG GTA -3'
F'	5' NH3-AAA AAA AAA ATA CCG TGA ACC TTA CCT GAT -3'
G	5'-AAA AAA AAA AGA GTA GCC TTC CCG AGC ATT-3'
G'	5' NH3-AAA AAA AAA AAA TGC TCG GGA AGG CTA CTC-3'
H	5'-AAA AAA AAA AAT TGA CCA AAC TGC GGT GCG-3'
H'	5' NH3-AAA AAA AAA ACG CAC CGC AGT TTG GTC AAT-3'
I	5'-AAA AAA AAA ATG CCC TAT TGT TGC GTC GGA-3'
I'	5' NH3-AAA AAA AAA ATC CGA CGC AAC AAT AGG GCA-3'
J	5'-AAA AAA AAA ATC TTC TAG TTG TCG AGC AGG-3'
J'	5' NH3-AAA AAA AAA ACC TGC TCG ACA ACT AGA AGA-3'
K	5'-AAA AAA AAA ATA ATC TAA TTC TGG TCG CGG-3'
K'	5' NH3-AAA AAA AAA ACC GCG ACC AGA ATT AGA TTA-3'
L	5'-AAA AAA AAA AGT GAT TAA GTC TGC TTC GGC-3'
L'	5' NH3-AAA AAA AAA AGC CGA AGC AGA CTT AAT CAC-3'
M	5'-AAA AAA AAA AGT CGA GGA TTC TGA ACC TGT-3'
M'	5' Cy3-AAA AAA AAA AAC AGG TTC AGA ATC CTC GAC-3'

* all oligonucleotides were synthesized by Integrated DNA Technology (IDT) and purified via high performance liquid chromatography (HPLC).

Table S2. Summary of antibodies used for macrophage experiments.

DNA label	**primary antibody (vendor)**	**secondary antibody (vendor)**
A'	mouse anti-hu IL-2 (BD Biosciences)	biotin-labeled mouse anti-hu IL-2 (BD Biosciences)
B'	mouse anti-hu MCP-1 (eBioscience)	biotin-labeled armenian hamster anti-hu MCP-1 (eBioscience)
C'	rat anti-hu IL-6 (eBioscience)	biotin-labeled rat anti-hu IL-6 (eBioscience)
D'	rat anti-hu GMCSF (Biolegend)	biotin-labeled rat anti-hu GMCSF (Biolegend)
E'	goat anti-hu MIF(R&D systems)	biotin-labeled goat anti-hu MIF(R&D systems)
F'	mouse anti-hu IFN-γ (eBioscience)	biotin-labeled mouse anti-hu IFN-γ (eBioscience)
G'	mouse anti-hu VEGF (R&D systems)	biotin-labeled goat anti-hu VEGF (R&D systems)
H'	mouse anti-hu IL-1β (eBioscience)	biotin-labeled mouse anti-hu IL-1β (eBioscience)
I'	rat anti-hu IL-10 (eBioscience)	biotin-labeled rat anti-hu IL-10 (eBioscience)
J'	mouse anti-hu IL-8 (R&D systems)	biotin-labeled mouse anti-hu IL-8 (R&D systems)
K'	mouse anti-hu MMP9 (R&D systems)	biotin-labeled goat anti-hu MMP9 (R&D systems)
L'	mouse anti-hu TNF-α (eBioscience)	biotin-labeled mouse anti-hu TNF-α (eBioscience)

Table S3. Digital data for the fluctuation in protein copy numbers for experiments with 1 cell in the chamber.

IL-2	MCP-1	IL-6	GMCSF	MIF	IFN-γ	VEGF	IL-1β	IL-10	IL-8	MMP9	TNF-α
3735.412	217395.9	13953.23	557.1622	3809515	13624.74	201.4036	8376.421	0	1454177	3205.591	152586.1
1665.362	27307.83	104.8926	1517.076	2820595	53647.16	22.99382	30393.38	2225.058	1549870	8513.336	139044.8
0	0	5.688741	983.9779	2039581	51073.18	5.659558	397.6828	1712.567	1556202	75864.65	105209.4
0	0	4.782456	0	442693.6	0	0.336728	0	0	341176.1	10460.81	39.82124
0	0	4.782456	0	394608.6	7158.123	0.336728	83.72112	0	1049468	5786.696	112.4533
0	9036.275	4.782456	315.5414	1182371	15521.45	2510.404	164.3377	0	2078531	530.3467	98.55574
0	8562.464	22.67125	1973.092	2340711	50886.57	0	8659.165	386.6576	1825752	3484.746	225206
972.853	5136.066	45.69175	0	2903862	30000.8	1.655758	1627.437	678.766	1357052	1609.678	487.7715
0	4625.892	5.688741	162.2633	515603.5	12411.14	258.1623	2951.517	1069.252	2085364	18909.8	95984.22
1115.354	5639.942	25.6359	0	3794851	59631.05	5.955249	75.74618	644.1138	829791.9	1197.849	9267.078
367.32	8562.464	0.620442	0	404940.8	0	5342.374	170.0894	425.4534	4964304	181518.4	2001.962
0	40152.21	47.5241	1517.076	3743529	8249.956	643.5375	2935.413	1281.727	5149720	38060.09	1084.421
876.3752	20185.95	28.71536	1658.653	665589.7	17294.07	4591.031	732.1417	1221.906	4543300	36619.56	127154.3
0	0	0	0	638485.4	0	0	2173.854	0	2932515	408789.6	64138.92
1068.126	0	13.28018	632.2731	438114.6	0	119.5423	102.6353	0	1034324	592.5651	4161.334
1575.52	19329.17	47.5241	961.4889	1217737	21180.92	2.07053	5.38982	813.5973	1055366	2244.563	1780.287
827.633	26895.82	175.1502	2258.346	5831647	64318.4	2721.671	3362.146	4140.063	3606621	5461.672	75502.9
0	4625.892	4.782456	256.7672	6562935	0	1.756733	8524.752	0	174775	2301.694	98.55574
0	0	18.45094	286.4852	359371.4	0	572.8267	52.38082	0	3107306	65788.63	25235.97
0	5136.066	0	371.9954	5772999	7715.093	0.919755	952.1023	125.4948	589949.5	3484.746	8.587119
577.7165	27307.83	7.645797	256.7672	481179.4	11991.4	5.082496	91.7772	1221.906	954720.5	1434.076	159.007
0	11362.51	218.9126	681.2702	3668936	35507.47	4.254203	3813.608	4117.263	2589890	42622.04	86305.23
474.0248	21038.24	6.64407	505.8466	396657.3	7715.093	1.859546	205.0206	0	8685444	1667.948	155173.2
0	0	336.0215	0	365278.4	0	0.606097	1608.84	174.4034	2065560	1138.365	3733.989
0	0	0	0	328035.4	7715.093	159.1543	138.7292	425.4534	1067345	3484.746	95.81771
0	0	58.9922	961.4889	300360.2	34353.44	0	54.93063	746.8858	1817495	2358.739	23134.31
0	0	4.782456	0	425186.2	7715.093	613.1612	99.90882	386.6576	4683202	3037.413	46.89755
0	0	3.928359	0	445991.3	7715.093	402.2585	0	975.2311	523909.4	6326.138	1054.297
2236.04	33403.67	476.1208	870.3418	435981.4	74992.86	23.9095	3930.914	1986.093	11697012	9358.114	8317287
0	8085.346	36.88775	453.3645	332604.1	11991.4	86.2306	113.6166	1370.279	1559706	7130.545	1958.179
1620.52	9974.818	0	286.4852	362920.9	7158.123	0.336728	42.31677	713.014	1569342	22053.76	23001.06
198.7022	28129.56	104.8926	582.4318	5431280	38632.32	0.534271	503.3473	746.8858	1414076	3818.009	82.34883
0	0	13.28018	0	294489.8	0	278.2761	39.8375	0	96873.01	181570.6	0
0	15851.76	13.28018	0	569708.6	11125.54	2369.121	328.8863	386.6576	1292647	23316.12	12607.48
1843.259	8562.464	86.41712	194.848	775007.6	19615.08	0.336728	4396.839	0	2386454	56608.75	570.4367
474.0248	16291.26	84.19013	870.3418	3567046	57034.26	44.96208	112244.6	1130.88	3238520	3707.119	85922.27
0	12275.83	14.52122	681.2702	446942.7	8249.956	3059.87	44.81139	425.4534	3127064	270629.6	16913.92
0	5639.942	65.01849	0	362459.2	0	0	16.1095	0	2971267	3429.024	115.2728
0	34605.82	175.1502	286.4852	499008.3	18309.28	152.4368	184.5588	425.4534	1011213	135792.6	1097.382
526.1976	584810	13.28018	0	308498.5	9264.625	483.3776	0	0	1509316	1052286	49352.54
421.1059	4625.892	0	531.6397	277526.7	17636.16	295.7684	824.1178	1684.681	1979177	42077.15	14565.16

924.7744	12275.83	114.5543	479.7625	451511.5	25255.09	1990.09	196.223	573.4616	2977232	121849.1	29473.5
0	0	5.688741	286.4852	1616413	24415.08	53.64644	21718.77	0	1961863	5948.816	16.0508
0	1935.839	22.67125	162.2633	537180.3	0	1.556662	426.2234	678.766	1662376	3928.711	1846405
4097.416	15410.74	6.64407	916.1621	627149.3	15153.07	950.0875	661.5037	911.38	4734071	15793.97	633893.1
0	5639.942	18.45094	0	3734680	19933.81	71.75808	611.5641	1877.786	1963379	160882.2	12793.76
0	0	45.69175	286.4852	472151	7715.093	188.2966	86.39776	0	2563383	70281.5	27115.65
138.713	12729.29	27.16157	128.1625	510521.3	9748.657	0.534271	363.1055	713.014	7637057	22154.85	306664.8
526.1976	14077.98	47.5241	753.3682	385982.2	17636.16	9497.397	81.05349	713.014	1650511	36569.86	69227.5
0	0	3.928359	505.8466	4597800	21486.18	55.44104	378.7795	0	4705311	1492.748	4042.245
474.0248	8562.464	13.28018	286.4852	415863.4	7158.123	0	304.2398	1656.69	6712149	124417.6	104764.8
0	4625.892	49.37952	870.3418	3610659	11125.54	308.8587	335.0802	1543.606	1731368	67269.56	273.0328
0	0	0	0	497690.4	12411.14	1.964157	57.49294	0	1609086	450905.5	109102.7
2149.562	10439.91	5.688741	286.4852	493432.2	0	95.38698	800.1525	0	2319845	933080.9	468816.9
0	2499.366	0	0	1938229	11563.1	15.08493	167.2109	1486.351	1882943	6809.424	1024.341
421.1059	260961.8	27.16157	1028.626	631535.9	0	297.85	213.8589	537.3803	1335228	1018.815	12.21319
0	7604.672	47.5241	194.848	414552.4	20562.75	3358.884	267.679	1656.69	4826026	12493.18	65787.75
778.5221	27307.83	339.5008	1638.592	3964841	84043.16	10.19566	170693.7	3082.111	4250173	17635.86	346394
0	4625.892	0	315.5414	480143.5	15521.45	401.1044	196.223	2225.058	3515798	580887	11928.38
0	8562.464	18.45094	286.4852	658884.1	7158.123	1.179999	150.0535	537.3803	1652656	454906.5	113008.1
474.0248	48688.48	15.79737	777.063	479056.9	15153.07	11.81997	621.5163	2039.74	4603005	201019.8	340191.5
474.0248	20612.64	6.64407	286.4852	436080.6	0	1.859546	234.6332	2012.957	6917958	11296.85	215980.3
0	0	768.0874	286.4852	373315	26079.52	1437.645	199.1509	678.766	2261670	2130.037	10466.12
0	0	0	0	426020.1	7158.123	2.743952	161.4698	0	3933389	4369.751	49058.97
0	0	189.3848	557.1622	494271.9	15521.45	494.498	127.5026	71.49773	3800164	477015.4	103268.1
1068.126	42500.29	5.688741	0	443142.7	0	2610.429	135.9132	220.2761	2342101	688400.6	12.21319
0	6631.472	19.82653	0	574020.6	12822.93	10.3724	175.8619	879.0676	4074696	105807.8	1513.189
972.853	10439.91	10.90809	729.5097	284256.4	18640.59	2235.697	133.1033	0	1470217	53399.89	4002.718
0	0	13.28018	0	597667.5	0	2019.485	264.6556	306.1297	1194410	29141.91	480.3807
0	51365.65	145.1361	1246.065	405806.5	32699.9	856.1518	113.6166	1959.145	1258039	183346.9	1417.034
0	729.7022	0	256.7672	602511.6	31733.5	0	234.6332	0	1122269	898.3988	400.546
1485.024	41719.38	139.8782	453.3645	444591	7158.123	885.0224	138.7292	1628.589	2793823	3540.416	27481.96
526.1976	6138.223	27.16157	0	465292.2	14400.48	1403.802	102.6353	746.8858	1844275	18451.63	97125.55
2192.854	60050.81	285.2598	557.1622	3976269	52552.65	235.1851	12868.12	1486.351	2056078	6272.314	6856.5
0	10439.91	0	128.1625	5629496	8249.956	0.399418	1762.11	678.766	813978.6	163717.2	92940.02
2535.544	14523.91	114.5543	344.0223	1484329	26621.01	8678.123	8057.573	2661.458	1986914	525123.6	889781.5
0	4108.532	0	557.1622	443841.6	7715.093	1.179999	216.8138	1281.727	1438747	72010.22	3496.753
421.1059	4625.892	55.08115	453.3645	533679.1	45692.16	1450.532	385.0693	463.4456	1859549	8089.271	175397.8
924.7744	0	27.16157	681.2702	2819971	22977.18	25.30396	258.6201	2836.369	2894811	40590.36	774.8536
1439.516	5136.066	47.5241	0	2087753	52000.61	0.399418	7422.418	879.0676	3000134	5786.696	97961.85
526.1976	0	0	162.2633	528450.2	11991.4	59.08624	22.98716	463.4456	1749215	3596.034	624.2794
577.7165	9506.996	49.37952	0	503131.4	15521.45	116.0933	837.8488	220.2761	1903608	164594.6	2006.839
577.7165	0	5.688741	453.3645	6660777	58080.71	120.3132	404.0062	0	1578115	1078.692	323.6175
0	11362.51	0	128.1625	440302	9264.625	114.9509	273.7368	813.5973	1578115	12129.72	1040989
1575.52	19329.17	325.6539	1638.592	4924300	64154.29	340.5053	1318.723	2861.155	2672000	23366.56	306.578

0	0	24.13892	0	6851805	53465.61	5.513485	638.1433	0	1028638	127948.9	12200.28
474.0248	9036.275	221.941	286.4852	458783.7	20873.14	49.24328	322.7051	1850.488	2457942	22811.51	822556.8
3613.793	57047.96	172.3469	938.885	406672.9	47264.38	865.9889	1690.864	2172.481	3502255	843555.9	353763.6
0	22308.79	60.97992	0	369312.3	19933.81	814.9924	119.1506	975.2311	2229100	92908.36	75331.28
2062.643	5639.942	0	194.848	828096.2	7715.093	3451.146	105.3695	463.4456	2062203	2529.389	49.30233
0	4625.892	150.4565	194.848	606027.9	15521.45	48.08955	732.1417	644.1138	2205137	44305.43	112117.4
876.3752	109736.4	15.79737	656.8714	4333366	13227.3	9.498279	3109.17	2910.581	1557792	40044.93	8399.296
474.0248	14077.98	58.9922	1050.792	4158207	40779.49	0.837598	2139.122	713.014	1602325	18247.85	13988.05
0	4625.892	9.77966	938.885	427984.9	28984.83	2539.309	133.1033	813.5973	3538045	6056.756	99712.96
474.0248	15851.76	97.82923	315.5414	3058525	52552.65	5.224942	344.3945	678.766	1596288	1434.076	17010.92
1620.52	30983.19	164.0253	2444.257	3783288	27421.74	8.150933	20591.01	713.014	1238515	126636.5	294604.8
0	5639.942	6.64407	0	4829314	14779.51	0	438.9771	0	8394607	1375.257	12.21319
0	9036.275	86.41712	1718.527	699222.5	0	0	8090.773	0	946538.8	1018.815	246.7378
421.1059	29356.69	57.02586	656.8714	427051.1	49758.73	5895.509	7.430834	713.014	855150.1	715.8439	12943.31
972.853	16729.29	124.4873	557.1622	3157311	24131.41	26.96196	2270.716	125.4948	1429803	10251.26	2675.917
474.0248	0	27.16157	344.0223	421026.8	33885.67	0.336728	158.6074	813.5973	4493846	3205.591	4785.501
0	0	4.782456	0	1735160	0	0	1064.458	1600.377	491041.6	56904.9	28.54088
924.7744	21462.78	329.098	1797.669	10572470	36640.69	87.27182	951072.8	2012.957	717967.5	5786.696	50463.01
1255.571	16729.29	36.88775	916.1621	387730.2	35507.47	12.37785	172.9731	943.4302	3107306	9305.439	99116.28
0	3047.191	0	0	601108.5	0	1098.532	62.65337	346.9365	1429264	2015.138	0
827.633	1935.839	22.67125	0	609026.5	16243.7	3776.053	49.844	644.1138	2839583	5948.816	10466.12
0	0	45.69175	0	529102.3	7715.093	148.7002	164.3377	0	2739500	135792.6	454.6833
0	5639.942	19.82653	800.6015	399905.3	11125.54	61.55719	99.90882	1069.252	3152475	3484.746	192.6131
1975.261	17165.9	322.2216	1203.28	10565748	90563.8	9.155434	41511.63	2959.817	2157535	136249.1	5338.093
0	0	18.45094	1246.065	476216.6	0	0.399418	1553.213	0	1844720	82939.55	2389.394
0	0	17.10759	531.6397	3728800	39283.39	2566.026	1008.095	0	747662.7	1667.948	230.5624
628.6544	9974.818	15.79737	426.6258	488669.7	30997.64	130.4801	65.2507	1038.132	4037787	39400.11	71229.18
924.7744	0	5.688741	0	1560874	36640.69	4.801319	54.93063	0	1778135	8724.937	77056.37
0	0	27.16157	0	382589.2	5961.002	1493.194	347.5054	0	1500979	607501.3	327.046
972.853	0	0	226.2736	441546.9	7715.093	786.2589	110.8603	678.766	7130236	167126.3	55851.67
526.1976	11362.51	3.130261	1203.28	1356636	21180.92	2759.997	3129.465	975.2311	2758719	3818.009	146319.6
577.7165	6631.472	19.82653	2201.941	5878268	13624.74	3241.913	37543.28	1221.906	1173170	13477.1	220.957
0	11362.51	0	315.5414	486844	27948.27	0	255.6081	463.4456	1388172	522389.9	78625.91
0	635058.1	6.64407	0	545876.8	7715.093	1100.19	190.3813	0	1518652	28391.09	109.6469
256.4187	46379.67	53.15834	729.5097	3301742	32699.9	4.389042	359.9795	1006.795	1864545	5353.088	227.3521
577.7165	13630.28	14.52122	2107.237	3806473	22683.47	121.4725	96650.04	1543.606	1174095	9252.748	26620.53
924.7744	10439.91	47.5241	453.3645	3281029	44088.98	0.016533	477.4821	346.9365	1063941	2812.305	447.3908
5587.157	5136.066	24.13892	681.2702	3016496	29240.69	47.22998	5719.854	425.4534	105126.8	6056.756	0
474.0248	8562.464	36.88775	1895.558	4112702	22683.47	3.224364	87695.31	644.1138	3622850	18094.94	112883.1
2955.955	18035.05	57.02586	2088.188	3559334	27421.74	17.95405	37266.68	1656.69	2244932	5786.696	952.3013
5355.51	8562.464	0	0	2892800	14015.67	128.5041	1271.685	0	1603673	9884.013	30912.89
0	0	14.52122	52.05951	831973.3	8249.956	518.8942	141.5514	0	1042440	1609.678	306814.1
0	4625.892	67.06888	557.1622	3166646	20249.67	2.288425	18257.35	71.49773	462439.1	2130.037	187929.7
5970.693	18035.05	90.92703	1160.163	2856820	31244.01	23.67953	522.8445	1795.612	215604.4	14560.51	4241.145

Table S4. Signal-to-noise ratio (S/N) for single cells in SCBC measurements

IL-2	MCP-1	IL-6	GMCSF	MIF	IFN-γ	VEGF	IL-1β	IL-10	IL-8	MMP9	TNF-α
1.0	4.7	3.6	1.4	1381.1	4.3	77.3	94.7	1.8	2622.4	119.5	410.7

Table S5. Parameters utilized for the protein assay calibration curve

	A1		A2		x0		p		Statistics	
	Value	Error	Value	Error	Value	Error	Value	Error	Reduced Chi-Sqr	Adj. R-Square
IL-2	0	0	256	0	7659.58168	973.0838	1.12824	0.16788	91.39131	0.99224
MCP-1	0	0	256	0	65733.51686	4770.5	1.12607	0.09607	29.62623	0.99578
IL-6	0	0	256	0	16231.59942	4515.94	0.67887	0.12265	243.09932	0.95697
GMCSF	0	0	256	0	2451.99685	295.3281	1.2195	0.13013	72.59138	0.99458
MIF	0	0	256	0	7892.74068	483.8218	1.14428	0.07578	20.31714	0.99821
IFN-γ	0	0	256	0	14549.5316	2773.804	1.57222	0.26181	172.2368	0.98713
VEGF	0	0	256	0	1687.9445	225.4782	0.69008	0.05631	58.49911	0.99513
IL-1β	0	0	256	0	2137.44388	208.9672	0.89593	0.07185	41.21361	0.99694
IL-10	0	0	256	0	3961.03661	328.4038	1.23209	0.08611	33.93572	0.99669
IL-8	0	0	256	0	1255.89317	225.9207	1.23262	0.19534	161.8703	0.98686
MMP9	0	0	256	0	70537.40022	1584.696	1.062	0.02495	2.60945	0.99961
TNF-α	0	0	256	0	4126.15703	661.2747	0.81683	0.09483	99.72583	0.99185

Table S6: Values of parameters used in simulation

Chamber size	2000 μm×100 μm ×18 μm
Cell diameter	10 μm
Diffusion Coefficient(11)	10^{-6} cm^2/sec
Protein secretion rate (MIF)	0.065 nM/min
Molecular weight	12500 Da

Table S7: The coefficients of variation for each of the assayed proteins from single cell experiments. The experimental CVs are estimated from the Monte Carlo simulations. The biological CVs, which clearly dominate the experiment, are calculated from $CV_{\text{assay}} = (CV^2{}_{\text{system}} + CV^2{}_{\text{biological}})^{1/2}$.

Barcode/Protein	Experimental CV (%)	Assay CV (%)	Biological CV (%)
B / MCP-1	7.12	380.4	380.3
E / MIF	7.05	55.2	54.7
F / IFN-γ	7.04	131.5	131.3
G / VEGF	7.03	149.7	149.5
H / IL-1β	7.02	300.6	300.5
J / IL-8	7.00	14.4	12.6
K / MMP9	6.98	192.6	192.5
L / TNF-α	6.97	132.9	132.7

Table S8: Digital representation of the covariance matrix for 1 cell measurements

COV	IL-2	MCP-1	IL-6	GMCSF	MIF	IFN-γ	VEGF	IL-1β	IL-10	IL-8	MMP9	TNF-α
IL-2	1.18E+06	-27830	7966.7	1.34E+05	2.30E+08	4.10E+06	85756	1.27E+06	1.60E+05	-1.06E+08	1.50E+07	2.31E+07
MCP-1	-27830	6.34E+09	-1.83E+05	-1.14E+06	-9.54E+09	-9.51E+07	6.10E+05	-3.31E+07	-2.52E+06	-8.51E+09	4.21E+09	-7.34E+08
IL-6	7966.7	-1.83E+05	9050.5	11507	1.56E+07	5.89E+05	734.25	4.20E+05	24714	-81623	-7.38E+05	1.04E+06
GMCSF	1.34E+05	-1.14E+06	11507	3.39E+05	3.75E+08	3.97E+06	53462	5.71E+06	2.07E+05	1.05E+07	-1.66E+07	1.75E+06
MIF	2.30E+08	-9.54E+09	1.56E+07	3.75E+08	3.12E+12	1.48E+10	-4.32E+08	1.19E+10	3.35E+08	-4.33E+11	-7.53E+10	-5.22E+10
IFN-γ	4.10E+06	-9.51E+07	5.89E+05	3.97E+06	1.48E+10	3.09E+08	-2.28E+05	1.40E+08	5.83E+06	-1.70E+09	-5.01E+08	-1.00E+08
VEGF	85756	6.10E+05	734.25	53462	-4.32E+08	-2.28E+05	2.48E+06	-2.65E+06	1.04E+05	9.34E+07	2.92E+07	2.59E+07
IL-1β	1.27E+06	-3.31E+07	4.20E+05	5.71E+06	1.19E+10	1.40E+08	-2.65E+06	4.78E+08	4.46E+06	1.86E+09	-4.08E+08	3.16E+08
IL-10	1.60E+05	-2.52E+06	24714	2.07E+05	3.35E+08	5.83E+06	1.04E+05	4.46E+06	7.39E+05	2.20E+08	-5.64E+06	2.92E+07
IL-8	-1.06E+08	-8.51E+09	-81623	1.05E+07	-4.33E+11	-1.70E+09	9.34E+07	1.86E+09	2.20E+08	2.73E+12	7.05E+09	3.56E+10
MMP9	1.50E+07	4.21E+09	-7.38E+05	-1.66E+07	-7.53E+10	-5.01E+08	2.92E+07	-4.08E+08	-5.64E+06	7.05E+09	3.70E+10	5.25E+09
TNF-α	2.31E+07	-7.34E+08	1.04E+06	1.75E+06	-5.22E+10	-1.00E+08	2.59E+07	3.16E+08	2.92E+07	3.56E+10	5.25E+09	5.26E+10

Supplementary Methods References

1. Fan, R., O. Vermesh, A. Srivastava, B. K. H. Yen, L. D. Qin, H. Ahmad, G. A. Kwong, C. C. Liu, J. Gould, L. Hood, and J. R. Heath. 2008. Integrated barcode chips for rapid, multiplexed analysis of proteins in microliter quantities of blood. Nature Biotechnology 26:1373-1378.
2. Shin, Y. S., H. Ahmad, Q. Shi, H. Kim, T. A. Pascal, R. Fan, W. A. Goddard, 3rd, and J. R. Heath. 2010. Chemistries for patterning robust DNA microbarcodes enable multiplex assays of cytoplasm proteins from single cancer cells. Chemphyschem 11:3063-3069.
3. Quake, S. R., and A. Scherer. 2000. From micro- to nanofabrication with soft materials. Science 290:1536-1540.
4. Millet, L. J., M. E. Stewart, J. V. Sweedler, R. G. Nuzzo, and M. U. Gillette. 2007. Microfluidic devices for culturing primary mammalian neurons at low densities. Lab on a Chip 7:987-994.
5. Lee, J. N., C. Park, and G. M. Whitesides. 2003. Solvent compatibility of poly(dimethylsiloxane)-based microfluidic devices. Anal Chem 75:6544-6554.
6. Levine, R. D. 2001. How large is 'large' for a thermodynamic-like behavior. Physica E 9:591-599.
7. Callen, H. B. 1985. Thermodynamics and an Introduction to Thermostatics. Wiley, NY.
8. Mayer, J. E., and M. G. Mayer. 1966. Statistical mechanics. Wiley, New York.
9. Alhassid, Y., and R. D. Levine. 1980. Experimental and Inherent Uncertainties in the Information Theoretic Approach. Chemical Physics Letters 73:16-20.
10. Bellman, R. 1970. Introduction to Matrix Analysis. McGraw-Hill, New York.
11. Han, Q., E. M. Bradshaw, B. Nilsson, D. A. Hafler, and J. C. Love. 2010. Multidimensional analysis of the frequencies and rates of cytokine secretion from single cells by quantitative microengraving. Lab on a Chip 10:1391-1400.